Aero-Thermo-Dynamic Analysis of a Low Ballistic Coefficient Deployable Capsule in Earth Re-Entry

G. Zuppardi, R. Savino and G. Mongelluzzo.

Department of Industrial Engineering – Aerospace Division
University of Naples "Federico II"
Piazzale Tecchio, 80 – 80125 Naples, Italy
zuppardi@unina.it

Abstract: The paper deals with a microsatellite and the related deployable recovery capsule. The aero-brake is folded at launch and deployed in space and is able to perform a de-orbiting controlled re-entry. This kind of capsule, with a flexible, high temperature resistant fabric, thanks to its lightness and modulating capability, can be an alternative to the current "conventional" recovery capsules. The present authors already analyzed the trajectory and the aerodynamic behavior of low ballistic coefficient capsules during Earth re-entry and Mars entry. In previous studies, aerodynamic longitudinal stability analysis and evaluation of thermal and aerodynamic loads for a possible suborbital re-entry demonstrator were carried out in both continuum and rarefied regimes. The present study is aimed at providing preliminary information about thermal and aerodynamic loads and longitudinal stability for a similar deployable capsule, as well as information about the electronic composition of the plasma sheet and its possible influence on radio communications at the altitudes where GPS black-out could occur. Since the computer tests were carried out at high altitudes, therefore in rarefied flow fields, use of Direct Simulation Monte Carlo codes was mandatory. The computations involved both global aerodynamic quantities (drag and longitudinal moment coefficients) and local aerodynamic quantities (heat flux and pressure distributions along the capsule surface). The results verified that the capsule at high altitude (150 km) is self-stabilizing; it is stable around the nominal attitude or at zero angle of attack and unstable around the reverse attitude or at 180 deg angle of attack. The analysis also pointed out the presence of extra statically stable equilibrium trim points.

keywords: deployable capsule aerodynamics; longitudinal stability analysis; plasma frequency; hypersonic rarefied gas dynamics; direct simulation Monte Carlo method.

Nomenclature

B = ballistic coefficient
C_D, C_{Mz} = drag, longitudinal moment coefficients
CG, Cp = gravity center, pressure center
D = open aero-brake diameter
e^- = electron charge
f_e = plasma frequency
g = gravity acceleration
h = altitude
I = stability index
Kn = Knudsen number
L = length
m = capsule mass
m_e = electron mass
M = Mach number
N = number density
p = pressure
$\dot{q}$ = heat flux
Q = thermal load
r = nose radius
R = trajectory curvature radius
Re = Reynolds number
s = curvilinear abscissa
S = surface

t = trajectory travel time
T = temperature
V = velocity
x_{cg} = position of the gravity center along the x-axis
x_p = position of pressure center along the x-axis

Greek symbols
α = angle of attack
γ = flight path angle
ε_0 = permittivity of vacuum
λ = mean free path
ρ = density

Subscripts, superscripts and special symbols
BCK = backward
CFD = Computational Fluid-Dynamics
DSMC = Direct Simulation Monte Carlo
e = electron
f = fluid-dynamic
FWD = forward
GPS = Global Positioning System
IMU = Inertial Measurement Unit
IRDT = Inflatable Re-entry Demostrator Technology
IRVE = Inflatable Re-entry Vehicle Experiment
max = maximum
mcs = mean collision separation
OBDH = On-Board Data Handling
ref = reference
s = simulated
TPS = Thermal Protection System
w = wall
∞ = free stream
(0) = stagnation point

1. Introduction

It is well known that a deployable, or umbrella like, re-entry capsule [1-4], thanks to lightness and to low construction and management costs, can be an alternative to the current "conventional" capsules. In fact, a deployable capsule is made of flexible, high temperature resistant fabric, folded at launch and deployed in space at the beginning of re-entry for de-orbit and for other re-entry operations. Reducing size, mass and power implies a significant reduction of launch costs and an increment of management capability, therefore of accessibility to space.

A key feature of such capsules is the low ballistic coefficient. This feature guarantees low peak stagnation point heating rate and temperature. As reported by Akin [5], the ballistic coefficient of a entry vehicle can be considered as a design parameter and not a consequence of other design requirements, like: the launch vehicle payload, influencing the mass, the aerodynamic configuration, influencing the drag coefficient, the launch vehicle diameter, influencing the reference area (typically the cross-section area). The possibility of changing the aero-brake geometry allows to properly adapt the ballistic coefficient to the flight conditions.

The present authors already analyzed the trajectory and the aerodynamic behavior of such a kind of capsule during Earth re-entry [3] and Mars entry [4]. In those studies, aerodynamic longitudinal stability analysis and evaluation of thermal and mechanical loads have been carried out in both continuum and rarefied regimes. Results verified that during the Earth re-entry for certain conditions the capsule can be aerodynamically self-stabilizing,, i.e. equilibrium is stable around the nominal attitude at zero angle of attack and is unstable around the reverse attitude at 180 angle of attack.

The present study is aimed at providing preliminary information about the aerodynamic behavior of a complete satellite system, including an orbital module and a re-entry module, equipped with a deployable adjustable aero-brake to control the de-orbiting phase and to thermally protect the payload during the atmospheric re-entry phase. It is assumed that a reversible deployment mechanism, including linear actuators, allows to adjust the rotation and the simultaneous elongation or shortening of the ribs, so that an umbrella can be closed or deployed to change aerodynamic drag and to

adjust the deorbit phase. During the atmospheric re-entry phase, after separation of the service module from the re-entry module, the aero-brake reduces velocity, allowing the capsule to maintain the inner payload at lower temperatures.

The present paper is focused on the aerothermodynamics of the orbital module and of the re-entry module, before and after separation of the service module, investigating local quantities (pressure, shear stress, heat flux) and global coefficients (lift, drag and longitudinal moment). Focal points were the evaluation of the longitudinal stability and of the plasma characteristics along the re-entry phase. The longitudinal stability can ensure that the satellite and the capsule do not assume, at high altitudes, wrong attitudes compromising the effectiveness of the system, since, in order to control the aerodynamic drag, the satellite axis has to be always aligned with the relative free stream velocity, with the forward stagnation point on the nose. This is a very important requirement considering that, during the orbital phase, if the system is aerodynamically stable in the suitable attitude, small size and relatively low power consuming reaction wheels and magneto-torques can be used for attitude control, especially in presence of large aerodynamic torques at lower altitudes. In addition, after separation of the service module from the re-entry capsule, the deployable re-entry system can not be equipped with an independent attitude control system and the correct attitude is only guaranteed if the system is aerodynamically stable. It is also important that the capsule has only one statically stable trim point (monostability), as reported by Chen et al. [6] who verified that a capsule configuration with secondary statically stable trim points is highly undesirable because it is extremely dangerous when a capsule stabilizes at the secondary trim point during re-entry because the payload could be exposed to the flow.

Hypersonic re-entry velocity creates a bow shock wave in front of the capsule, producing dissociation and ionization of air. The plasma layer, surrounding the capsule, can cause communication interference or blackout, especially to the Global Positioning System (GPS). Therefore, the evaluation of the plasma frequency is important, even though it is not relevant in terms of heat flux. Furthermore, since electrical connections between the service module and the capsule must be ensured by umbilical electrical connectors, after the capsule separation from the platform, connector pins can be exposed to the ionized layer enveloping the capsule during re-entry into the Earth atmosphere. Knowledge of the concentrations of charged particles, in particular positive ions and free electrons, together with a number of neutral particles, can be important to evaluate the possibility to generate variations in the electrostatic potential of the spacecraft surface, with respect to the surrounding plasma environment, and/or potential variations among different portions of the spacecraft that can affect the proper functioning of electric or electronic instruments.

Since both the stability and the black-out problems occur at high altitude, computer tests were carried out in rarefied flow fields, therefore the use of Direct Simulation Monte Carlo codes was mandatory. Computation, in continuum or at low altitude ($\leq$50 km) of the drag coefficient, needed for the tracing of the re-entry trajectory (Sec.3), was carried out for a very similar capsule by Iacovazzo et. al. [3] by means of a Computational Fluid-Dynamics (CFD) code; for this reason, the same values of drag coefficient were also considered in the present paper.

2. Re-entry demonstrator configuration

Figure 1 shows the outline of the satellite in deployed configuration. The complete satellite, including service module and re-entry module, is a cylinder with 30 cm diameter and total length of 62 cm. The solid lines identify the re-entry module (length 38 cm), the dashed lines identify the service module (length 24 cm). The re-entry module also includes a rigid hemispherical nose (7 cm thick, with a radius at the stagnation point of 19.5 cm). The re-entry module contains the payload and other subsystems needed for the mission, umbrella-like framework, ceramic fabric for the conical deployable aero-brake and a light-weight, temperature-resistant material (e.g. carbon fiber composites) for the rigid hemispherical nose. Other subsystems include, for instance, linear actuators, batteries, sensors, recovery systems in the re-entry module, as well as On-Board Data Handling (OBDH), power, telecommunication, attitude control systems, thermal control systems in the service module. A total mass of 15 kg and 35 kg was assumed for the re-entry and service modules, respectively.

When completely deployed, the aero-brake is a half cone of 45 deg and a maximum diameter (D) of 104 cm. The drag and the moment coefficients are computed considering as reference area (S) the base area (8494.6 or 706.8 cm^2, depending on the configuration) and as reference length the diameters of the deployed aero-brake and of the satellite (104 or 30 cm). Table 1 summarizes some parameters of the re-entry demonstrator. The reference system was assumed according to Fig. 1, with the z-axis forming a right-handed triad with the longitudinal x-axis and the radial y-axis.

It has to be pointed out that there is no ideal shape for such a kind of capsule because many aspects influence its design like aerodynamic stability, heating, functionality, etc. Many sphere-cone aero-brake configurations exist whose aperture angle can be up to 60 deg. The 45 deg aperture angle is typical of low ballistic capsules both for Earth and for interplanetary missions [7] and it is a compromise between an efficient aerodynamic deceleration (the higher the angle the stronger the deceleration) and longitudinal stability (the higher the angle the less stable the equilibrium). For the present capsule, the cylindrical shape provides a good solution for the link and the detachment of the service module, the aero-brake deployment mechanics and the housing in the launcher ogive.
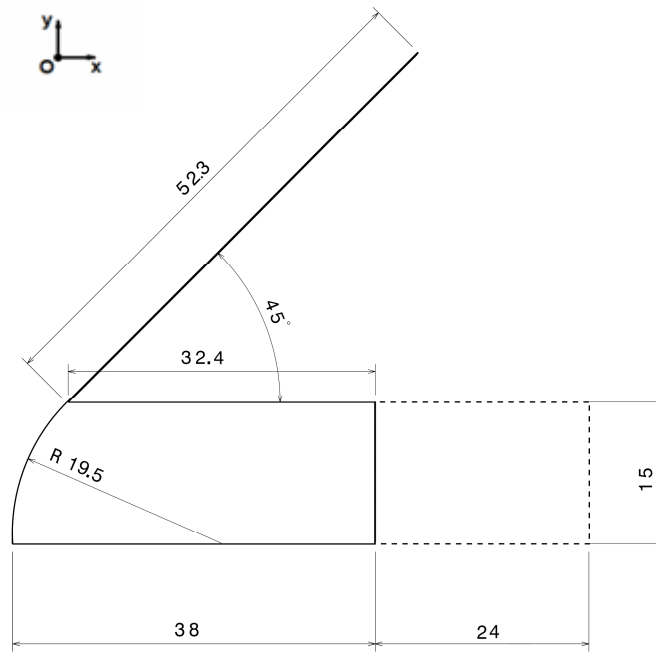
Fig. 1. Geometrical characteristics of the re-entry demonstrator (dimensions are in centimeters)

Table 1: Parameters of the re-entry demonstrator

Cylinder length [cm]	$38 \div 62$
Cylinder diameter [cm]	30
Mass [kg]	$15 \div 50$
Aero-Brake diameter [cm]	104
Reference surface [cm^2]	$707 \div 8495$
Nose radius [cm]	19.5
Reference length [cm]	$30 \div 104$

3. Re-entry Trajectory

Equations 2.a and 2.b compute the trajectory of the capsule after its separation from the satellite:

$$\frac{dV}{dh} = \frac{1}{2}\frac{\rho V}{\sin\gamma}\frac{SC_D}{m} - \frac{g}{V} \tag{2.a}$$

$$\frac{d\gamma}{dh} = \frac{1}{R\sin\gamma} - \frac{g}{V^2}\frac{1}{tg\gamma} \tag{2.b}$$

where V is velocity, γ is flight path angle, C_D is drag coefficient, S is reference area (i.e. the capsule base area), m is capsule mass, g is gravity acceleration and R is curvature radius of the trajectory. The inverse of the ratio SC_D/m is defined as ballistic coefficient (B [kg/m^2]). Pressure at the stagnation point of the capsule (p(0)) was preliminary evaluated assuming a pressure coefficient of 2, thus:

$$p(0) \cong \rho V^2 \tag{3.a}$$

whereas stagnation point convective heat flux ($\dot{q}(0)$) was evaluated by the Tauber's engineering formula [8]:

$$\dot{q}(0) = 1.83 \times 10^{-4} \sqrt{\frac{\rho}{r}} V^3 \tag{3.b}$$

where r is curvature radius of the capsule nose at the stagnation point. Equation 3.b provides an engineering estimation of heat flux. More precise values were computed by DSMC (see Sec.6).

Equations 2.a and 2.b were integrated numerically by a forward scheme with a first order approximation (Euler method). The following Eq. 4 computes the thermal load at the stagnation point $Q(0)$:

$$Q(0) = \int_0^t \dot{q}(0) dt \tag{4}$$

where t is the trajectory travel time.

4. Direct Simulation Monte Carlo (DSMC) Codes

It is well known that the Direct Simulation Monte Carlo (DSMC) method [9, 10, 11] is currently the most widely used tool for the solution of rarefied flow fields from continuum low density (or slip flow) to free molecular regimes. DSMC considers the gas as made up of discrete molecules. It is based on the kinetic theory of gases and computes the evolution of millions of simulated molecules, each one representing a large number (say 10^{15}) of real molecules in the physical space. Intermolecular and molecule-surface collisions are taken into account. The computational domain is divided in cells, used both to select the colliding molecules and to sample the macroscopic, fluid-dynamic quantities. The most important advantage of the method is that it does not suffer from numerical instabilities and does not directly rely on similarity parameters (i.e. Mach and Reynolds numbers). On the other hand, it is inherently unsteady. A steady solution is achieved after a sufficiently long simulated time.

The DSMC codes used in the present study are: 2-D/axial-symmetric DS2V-4.5 64 bits [12] and 3-D DS3V-2.6 [13]. DS2V can consider, optionally, two built-in chemical models by Gupta-Yos-Thompson [14] for air. A model considers air as made up of five neutral species (O_2, N_2, O, N and NO) and 23 chemical reactions, the other model considers air as made up of ten reacting species (O_2, N_2, O, N, NO, O^+_2, N^+_2, O^+, N^+, and NO^+) and 45 chemical reactions. This code was utilized to study the aerothermodynamic behavior of the axial-symmetric capsule, with its deployed aero-brake, during atmospheric re-entry. DS3V implements only the first Gupta-Yos-Thompson model. The three-dimensional model was utilized to study the aerodynamic stability of both the complete satellite and the re-entry capsule after separation.

Both codes are "sophisticated". As widely reported in literature [15, 16, 17], a DSMC code is defined sophisticated if it implements computing procedures able to guarantee a higher efficiency and accuracy with respect to a "basic" DSMC code. A sophisticated code, in fact, considers two sets of cells (collision and sampling cells) with the related cell adaptation, and implements methods promoting nearest neighbor collisions. This type of code automatically generates computational parameters such as number of cells and of simulated molecules by the input numbers of megabytes and of free stream number density. It uses a radial weighting factor in solving axial-symmetric flow fields and provides optimal time step. Finally, the same collision pair cannot have sequential collisions; this is physically impossible because after a collision, the molecules move away in opposite directions.

Besides being sophisticated, these codes are also advanced; the user can verify that the numbers of simulated molecules and of collision cells are adequate by means of the online visualization of the ratio between the molecule mean collision separation (mcs) and the mean free path (λ) in each collision cell. In addition, the codes allow the user to change (or to increase) the number of simulated molecules during the run. The mcs/λ ratio has to be less than unity everywhere in the computational domain. Bird [15] suggests 0.2 as a limit value for an optimal quality of the run. In addition, the code gives the user information about the stabilization of the runs by means of the profile of the number of simulated molecules as a function of the simulated time. The stabilization of a DSMC calculation is achieved when this profile becomes jagged and included within a band defining the standard deviation.

5. Test Conditions and Quality of the Results

The re-entry trajectory was computed from 170 km. The initial conditions are: V_∞=7800 m/s, γ=0, 2, 4 or 6 deg and C_D=1, the latter constant along the whole trajectory. A subsequent computation of the trajectory relies on variable drag coefficient as function of altitude. The environmental parameters at each altitude were calculated by a computer version of the US Standard Atmosphere 1976. Tables 2 and 3 report some input data and free stream parameters for the 3-D and

2-D DSMC simulations, respectively. Velocity and related parameters (M_∞, $Re_{\infty D}$) are those computed by Eq.2.a and 2.b with $\gamma=0$ deg. According to Moss [18], the capsule in deployed configuration is in transitional regime: $10^{-3}<Kn_{\infty D}<50$.

The 3-D runs were performed by DS3V at the altitude of h=150 km and in the angle of attack interval of 0-180 deg, with a 5 deg spacing, for the evaluation of the capsule longitudinal stability. The 2-D runs were performed by DS2V for the evaluation of the capsule drag coefficient along the re-entry path.

Table 2: Input data and free stream parameters in rarefied flow for DS3V simulations

h [km]	V_∞ [m/s]	N_∞ [m^{-3}]	T_∞ [K]	M_∞	$Re_{\infty D}$	$Kn_{\infty D}$
150	7800	5.15×10^{16}	634	13.3	0.42	47.8

Table 3: Input data and free stream parameters in rarefied flow for DS2V simulations

h [km]	V_∞ [m/s]	N_∞ [m^{-3}]	T_∞ [K]	M_∞	$Re_{\infty D}$	$Kn_{\infty D}$
130	7800	1.94×10^{17}	468	16.6	2.4	1.0×10^{1}
110	7800	2.14×10^{18}	244	24.0	48	7.1×10^{-1}
100	7735	1.19×10^{19}	196	27.2	339	1.2×10^{-1}
95	7632	2.92×10^{19}	189	27.5	857	4.6×10^{-2}
88	7293	1.01×10^{20}	187	26.5	2910	1.3×10^{-2}
83	6843	2.37×10^{20}	193	24.5	6270	5.6×10^{-3}
78	6263	5.25×10^{20}	203	19.7	10951	2.6×10^{-3}
73	5233	1.12×10^{21}	212	17.9	20850	1.2×10^{-3}
68	4109	2.27×10^{21}	225	13.6	31645	6.1×10^{-4}

The DS3V and DS2V runs were carried out with a number of simulated molecules of about 9.0×10^{6} and 2.0×10^{7}, respectively. For all runs, the codes suggested a number of 6 molecules/cell for the adaptation process of the collision cells, while, for the sampling cells, DS3V suggested a number of 30 molecules/cell, DS2V suggested a number of about 250 molecules/cell.

Besides from the above mentioned DSMC criterion (see Sec. 4), the stabilization of the runs was also verified from a fluid dynamic point of view by means of the ratio of the simulated time (t_s) to the fluid-dynamic time (t_f), which is the time needed to cross the computing region at the free stream velocity. A rule of thumb suggests that a fluid-dynamic computation is reasonably stabilized when $t_s/t_f \cong 10$. As reported in Table 4, even though the value of mcs/λ for the 2-D runs does not always satisfy the suggested limit value of 0.2, it is less than unity up to the altitude of 73 km, as requested by the method, and it is only slightly higher than 1 at h=68 km. Moreover, the ratio t_s/t_f satisfies the stabilization criterion of the runs from a fluid-dynamic point of view. These criteria are even more satisfied at altitudes higher than 100 km, therefore the parameters at such altitudes are not reported in Table 4. All 3-D tests satisfy the quality requirements. As an example, Table 5 reports typical values of both parameters, that do not significantly change in the whole interval of angles of attack.

Table 4: Quality parameters for the DS2V runs

h [km]	100	95	88	83	78	73	68
mcs/λ	0.007	0.018	0.07	0.18	0.42	0.61	1.31
t_s/t_f	10.08	9.62	23.79	19.03	14.70	10.05	6.60

Table 5: Quality parameters for the DS3V runs

h [km]	150
mcs/λ	0.03
t_s/t_f	50.00

6. Analysis of the results

6.1 2-D tests

Two-dimensional computations were carried out by the DS2V code to study the aerothermodynamic behavior of the re-entry capsule, in deployed configuration, after separation from the service module, during its descent into the dense

atmosphere. As said before, for a preliminary analysis, the aerodynamic drag coefficient used in Eq. 2.a and 2.b was assumed equal to 1 along the whole trajectory. The computation of the trajectories was then corrected using drag coefficients computed by DS2V at the altitudes reported in Table 3 and by Iacovazzo [3] at altitudes between 10-50 km. The drag coefficient was assumed 0.75 for altitudes less than 10 km and 2.05 for altitudes higher than 130 km while it was calculated by the following equation, in the altitude interval $10 \leq h \leq 130$ km. Figure 2(a) shows the drag coefficient profile and the related best fit curve:

$$C_D = 0.8432 - 4.7193 \times 10^{-3}h + 1.3510 \times 10^{-4}h^2 - 1.7869 \times 10^{-7}h^3 \tag{5}$$

where altitude h is in kilometers. The correlation coefficient is 0.9858. Figure 2(b) shows the profile of the ballistic coefficient B [kg/m^2] as a function of altitude. B is very low, compared with the ballistic coefficient of the current re-entry capsules: B ranges from 8 to 22 in the interval 10-130 km. As reported by Akin [5], typical values of the ballistic coefficient range from 250 to 500 kg/m^2. For example, the Dragon V1 capsule (m=3310 kg, S=10.8 m^2) [19], re-entering from the International Space Station and assuming a drag coefficient of 1, has a ballistic coefficient of 308. The very low value of B computed for the present capsule is due to its small dimensions (30 cm diameter with closed aero-brake, 104 with open aero-brake); however, similar capsules of larger dimensions, both deployable or inflatable, still have low ballistic coefficients. In fact, deploying or inflating the aero-brake involves a surface increase with no mass increment.
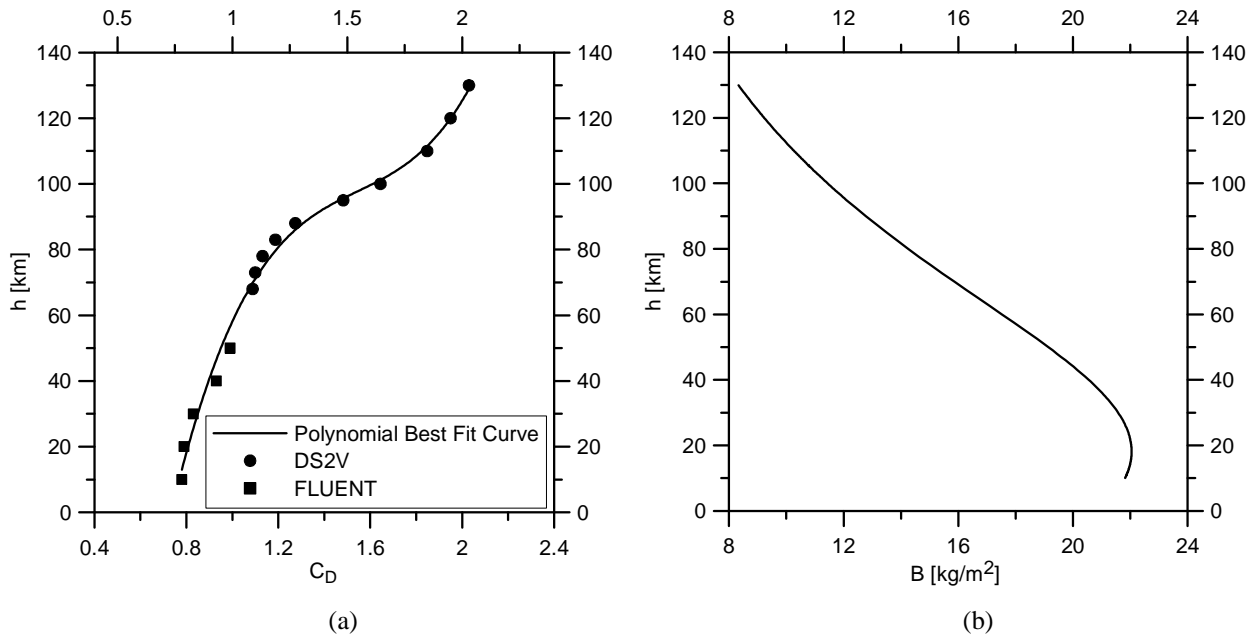

(a)   (b)

Fig. 2 – Profiles of (a) drag coefficient, with related polynomial best fit curve (α=0 deg), and (b) ballistic parameter as functions of altitude

Figures 3(a) to 3(d) show the profiles of velocity (a), Mach number (b), stagnation point pressure (c) and stagnation point heat flux (d) along the four re-entry trajectories, computed with variable drag coefficient and with four different re-entry angles: γ=0, 2, 4 and 6 deg. Table 6 reports the travel time of the trajectories, the maximum values of pressure and heat flux, plus the thermal load. Both pressure and heat flux increase with the flight path angle; the values at γ=6 deg are more than double than the ones at γ=0 deg. The maximum values of these quantities are met between h=60 and 80 km. Even though the maximum heat flux at the stagnation point increases with γ, the heat load decreases because the travel time of the trajectory decreases.

Table 6: Maximum values of stagnation point pressure and of heat flux, heat load

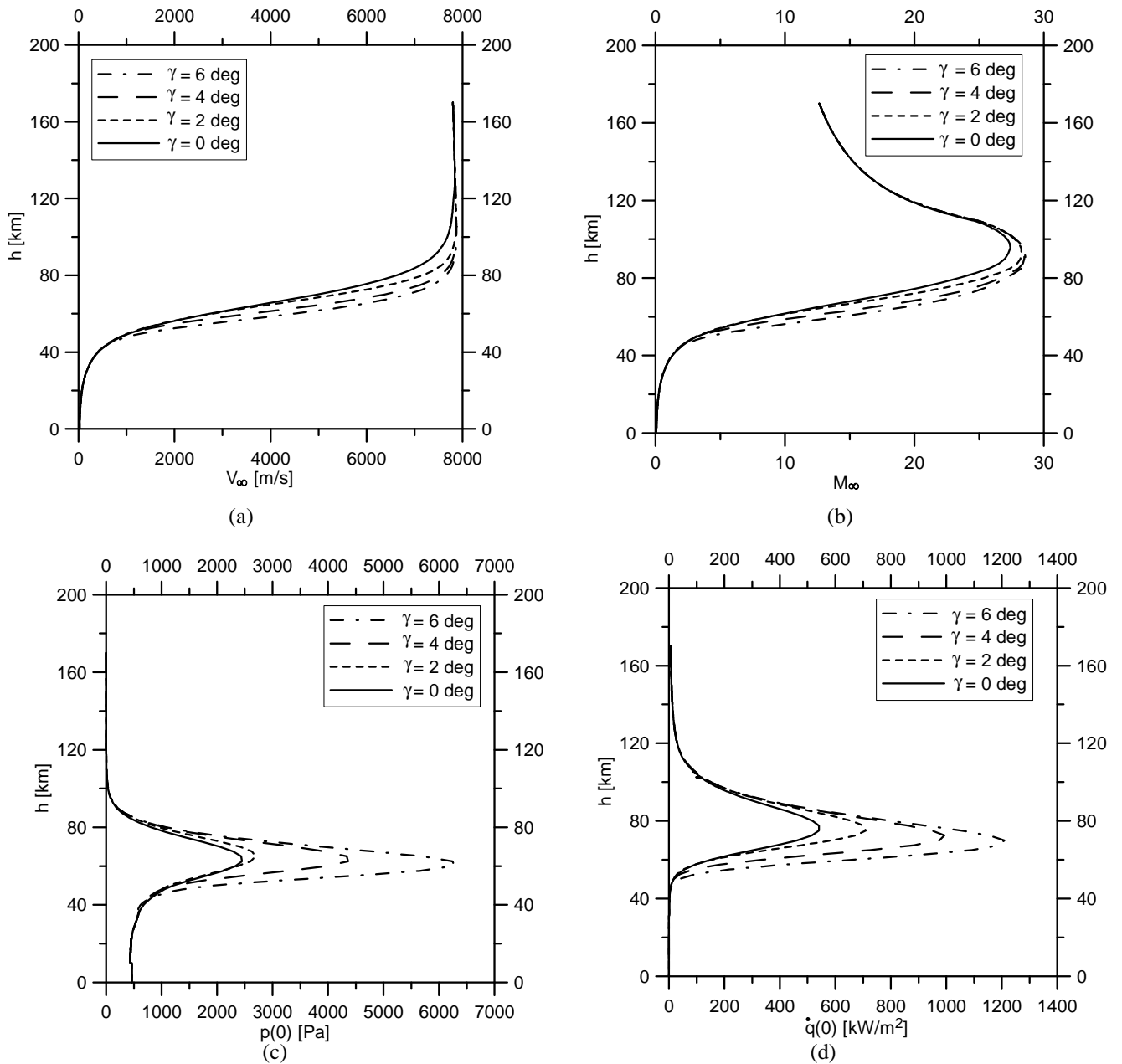| γ [deg]	t [min.]	p_{max} [Pa]	$\dot{q}(0)_{max}$ [kW/m^2]	Q(0) [kJ/m^2]
0	80	2447	541	112
2	21	2696	710	82
4	18	4360	993	62
6	16	6268	1209	52

Fig. 3 - – Influence of flight path angle on the profiles of (a) velocity, (b) Mach number, (c) stagnation point pressure and (d) stagnation point heat flux along the four computed re-entry trajectories

Figures 4(a) and (b) show the profiles of pressure and heat flux at the capsule stagnation point as a function of altitude, computed by the DS2V code. The free stream velocity used in the computations, reported in Table 3, is related to the re-entry path angle of 0 deg.

While conditions at the stagnation point are not critical, because of the presence of the thermal resistant rigid hemispherical nose (see Sec.2), information about pressure and heat flux on the aero-brake (made up of fabric and supporting ribs) can be relevant. In order to verify the resistance of the aero-brake to both the aerodynamic and the thermal loads, Fig.5(a) and (b) show the pressure profile and heat flux along the aero-brake surface at the altitude of 78 km where heat flux meets a maximum value (see Fig.4(b)). The shear stress is negligible; its maximum value is 61 Pa compared to 1375 Pa for pressure. The influence of chemical (dissociation, vibration, etc.) and ionization reactions was also evaluated; the capsule surface was considered non-catalytic and at a wall temperature of 300 K. Both figures clearly show that the influence of ionization on heat flux is negligible, while the influence of chemical reactions is pretty relevant. Considering that a possible fabric is the 3M NEXTEL, whose maximum operating temperature is around 1500 K and that the supporting ribs can be made of Titanium, thermal and mechanical aero-brake resistance requirements should be satisfied.
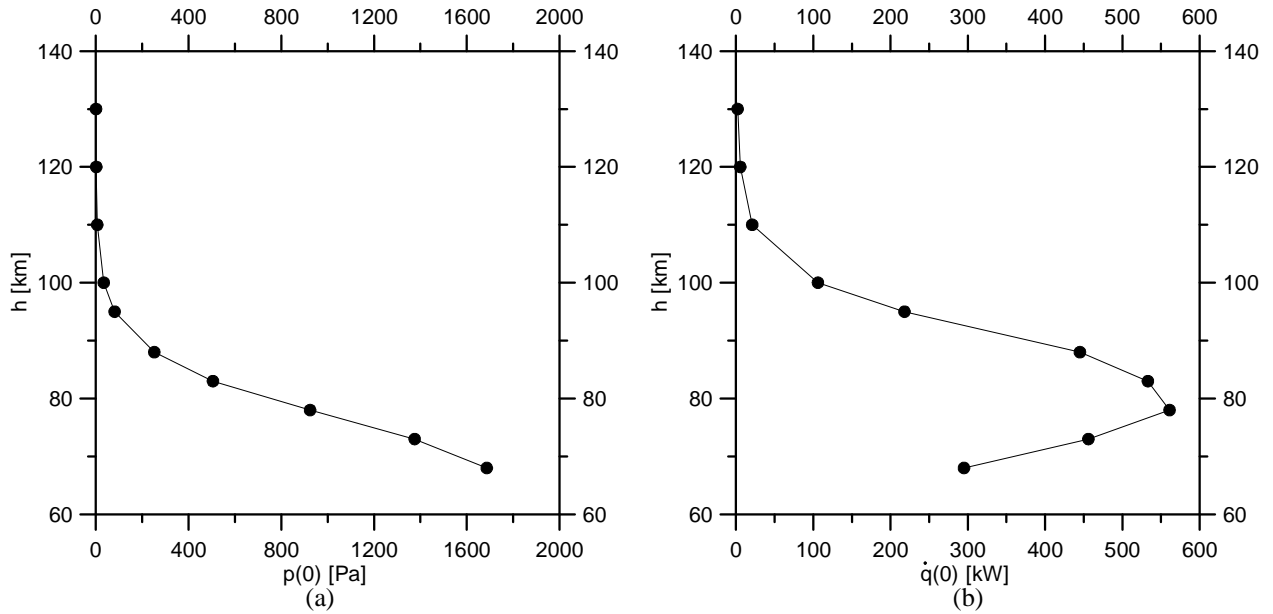
Fig. 4 – Profiles of pressure (a) and heat flux (b) at the capsule stagnation point as functions of altitude
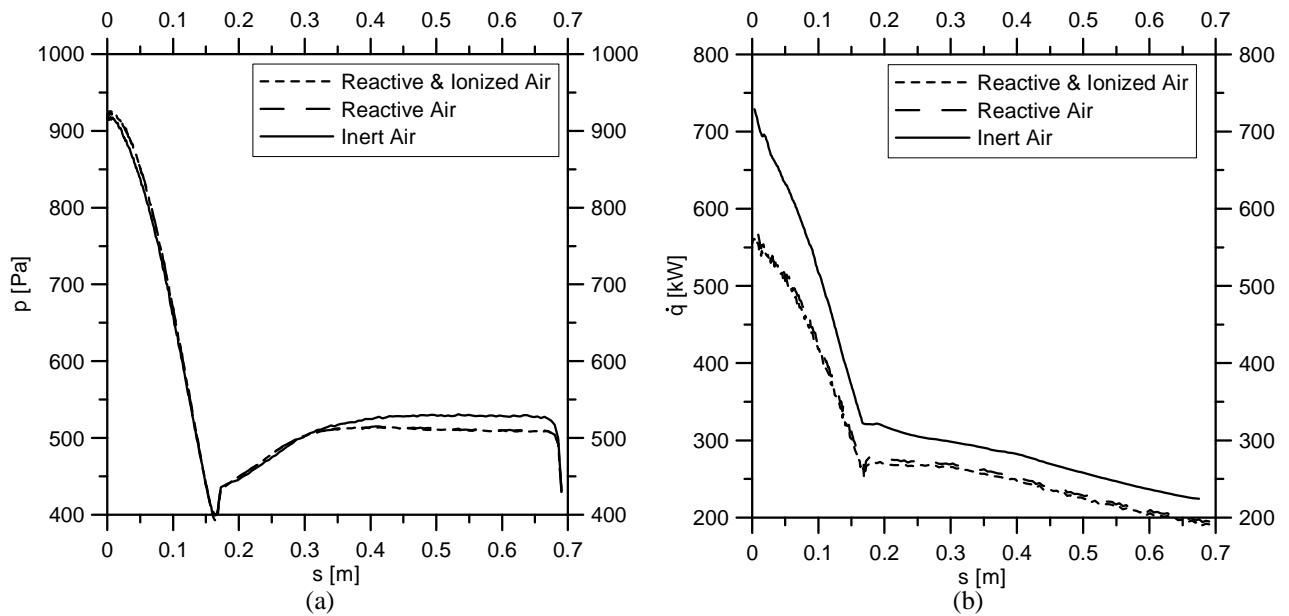

Fig. 5 – Profiles of pressure (a) and heat flux (b) along the capsule surface by three chemical states of air: h=78 km

As well known, local stiffness effects, such as circumferential and axial modes, are strongly dependent on the material stiffness, aero-brake or TPS boundary conditions and dimensions (e.g. thickness). Since the purpose of the present study is to assess the aerodynamic field in rarefied regime, it was supposed that the stiffness of the structure is high enough to not deal with flutter effects. The aeroelastic deformation was not considered because it requires an iterative calculation scheme that involves aerodynamics and structure, but it will be the subject of future work.

Furthermore, due to the different configurations, it is not possible to compare a deployable aero-brake (such as the structure presented in this work) with an inflatable TPS (such as the IRDT or the IRVE) in terms of vibration behavior. However, there are some works [20, 21] that show how the ratio of the radius of the conical shell to the TPS length influences the flutter behavior of a conical shell. As shown in [20, 21] for simple cases (simply supported and single layered TPS), the flutter behavior is strongly dependent on the material mechanical and geometric properties of the TPS (such as thickness, bending stiffness, BCs, etc). For larger dimensions (corresponding to larger capsules) the structure should be more flexible but, as well known, in dynamic aero-elasticity the essential point is the coupling between the unsteady aerodynamic forces and their structural modes.

The plasma frequency (f_e [GHz]) is related to the number density of electrons around the capsule and is computed by the following formula, reported by Kim et al. [22]:

$$f_e = \frac{1}{2\pi}\sqrt{\frac{(e^-)^2 N_e}{\varepsilon_0 m_e}} = 9\sqrt{N_e} \times 10^{-9} \tag{6}$$

where N_e [m^{-3}] is the number density of electrons, e^- is the electron charge, ε_0 is the permittivity of vacuum and m_e is the electron mass. In the present application N_e was approximated by the sum of the number density of cations of all species (O_2^+, N_2^+, O^+, N^+, NO^+) that impacted the capsule surface. Since DS2V considers the gas globally neutral from an electrical point of view, the number of cations is equal to that of electrons. As an example, Fig 6(a) shows a polynomial (third order) best fit curve of the electron number density along the capsule surface at h= 78 km. In the present application N_e, used in Eq.6, was the average value on the capsule surface.

According to Kim [22], the GPS black-out occurs in the range of plasma frequency 0.3-3 GHz. Assuming the intermediate limit value of 1.65 GHz, fig. 6(b) shows that the plasma frequency overcomes the limit value in the altitude interval 70-85 km, approximately, and that the maximum plasma frequency altitude is 78 km. Since this issue is crucial for the success of a mission, the analysis was enhanced, at this altitude, considering the effect of possible errors of the free stream velocity (therefore of the capsule kinetic energy) on the air ionization level and then on the plasma frequency. The effects of ±10% variations of the computed velocity (in this case 5637 and 6889 m/s) is relevant; it involves variations of about -60% and 90% of the plasma frequency, respectively.
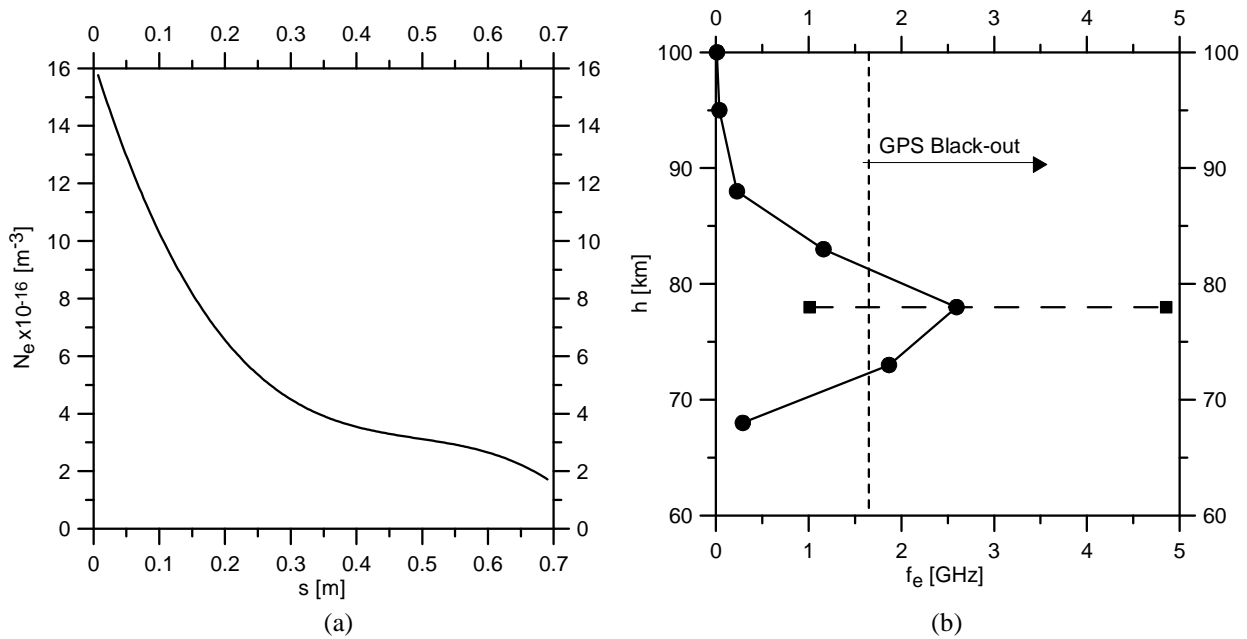

(a)   (b)

Fig. 6 – Polynomial best fit curve of the electron number density along the capsule surface at h=78 km (a) and profile of the plasma frequency as functions of altitude (b)

6.2 3-D tests

Three dimensional computations were carried out by the DS3V code on three system configurations: i) service module with attached re-entry module and closed aero-brake, identified in the figures as "closed satellite", ii) service module with attached re-entry module and open aero-brake, identified in the figures as "open satellite", iii) re-entry module with open aero-brake, identified in the figures as "open capsule". In order to compare the drag and the longitudinal moments for the three configurations, the results are presented as dimensional for less than the dynamic pressure. More precisely, they are shown in terms of $C_D S_{ref}$ and $C_{Mz} S_{ref} L_{ref}$. L_{ref} and S_{ref} are the reference length and the reference surface, respectively; L_{ref} and S_{ref} are the diameter and the base area of the deployed aero-brake for the "open satellite" and "open capsule" configurations, the diameter and the surface of the base of the cylinder for "closed satellite" configuration. Considering that the beginning of the re-entry is the most delicate phase and that the service module separates from the capsule at h=150 km, the analysis was carried out only at this altitude.

To verify the influence of the configurations on Aerodynamics, or of the length of the cylinder, figures 7(a), (b) and (c) show 3-D maps of pressure on the capsule surface for the "open satellite" configuration, for example at three angles of attack: 0, 45, 90 deg, respectively. The positions of the gravity center (CG) and of the pressure center (Cp) are shown

in the same figures. The position of the pressure center along the x-axis moves forward with the increase of the angle of attack; it moves from 0.2 m at α= 45 deg to 0.13 m at α= 90 deg, almost overlapping the gravity center. As shown in Fig.7(c), at α= 90 deg the service module is exposed to the flow. This alters the position of the center of pressure and therefore the size of the moment, and increases the drag.

In order to quantify the influence of the service module on the longitudinal moment, Table 7 reports the stability index I ($I=(x_{cg}-x_p)/L_{ref}$) for the "open satellite" and "open capsule" configurations. The index is slightly higher for the "open capsule" configuration. This is probably due to a backward movement of the pressure center higher than the supposed backward movement of the position of the gravity center. This verifies that the service module produces a destabilizing effect. Fig.8 shows the profiles of drag for the three configurations. The presence of the service module increases the drag. For example at α=90 deg, $C_D S_{ref}$ increases from 0.58 to 0.67 [m^2].
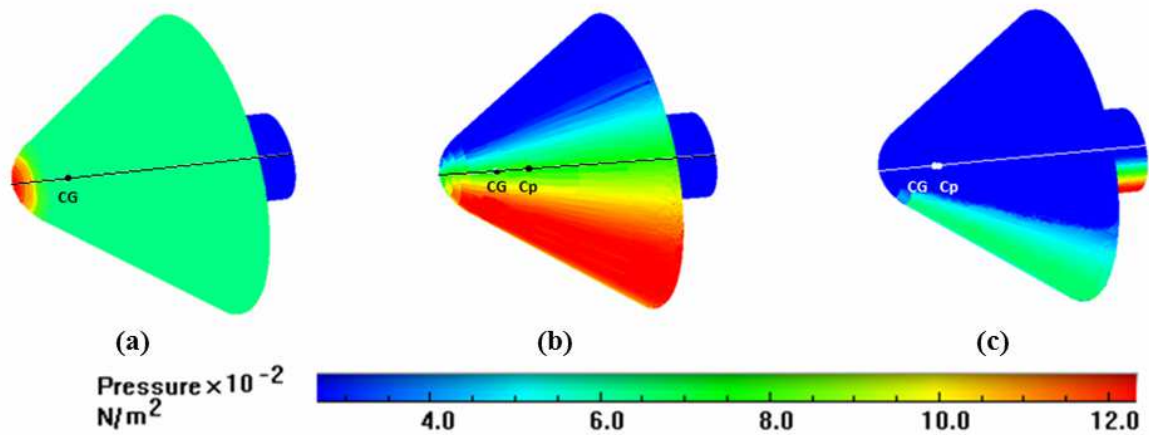

Fig.7 – Pressure 3-D maps on the capsule surface at (a) α=0 deg, (b) α=45 deg and (c) α=90 deg: h=150 km

Table 7: Stability Index for two configurations

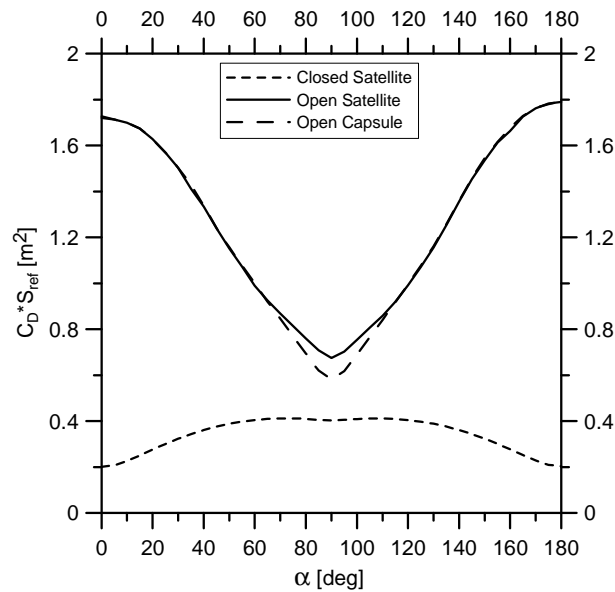| α [deg]	"open satellite"		"open capsule"	
	x_{cg} [m]	I	x_{cg} [m]	I
150	0.125	0.4247	0.100	0.4269
	0.250	0.4244	0.200	0.4269
	0.375	0.4242	0.300	0.4269
160	0.125	0.4240	0.100	0.4266
	0.250	0.4199	0.200	0.4267
	0.375	0.4253	0.300	0.4266
170	0.125	0.4244	0.100	0.4260
	0.250	0.4243	0.200	0.4267
	0.375	0.4243	0.300	0.4261

Fig. 8 – Profiles of the capsule drag for the three configuration: h=150 km

Taking into account the reference system shown in Fig.1, a negative longitudinal moment indicates a nose-down pitching moment. Thus, the condition $C_{Mz}=0$ identifies a longitudinal equilibrium, while a negative value of the derivative $dC_{Mz}/d\alpha$ identifies a stable equilibrium; the more negative the derivative, the more stable the equilibrium.

The positions of the moment reduction pole, identifying possible positions of the gravity center (x_{cg}) along the axis, are: 0.125 m, 0.250 m and 0.375 m for the "open satellite" and "closed satellite" configurations and 0.1 m, 0.2 m, 0.3 m for the "open capsule" configuration. Figures 9(a), (b), (c) show the profiles of C_{Mz} as functions of the angle of attack in the interval 0-180 deg. Figures clearly verify that:

i) when the aero-brake is open, the capsule is stable in forward (FWD) attitude (i.e. around zero angle of attack), and is unstable in backward (BCK) attitude (i.e. around 180 deg angle of attack), for every position of the pole. On the contrary, when the aero-brake is closed, this behavior is met when the position of the pole is not rearward, for example $x_{cg}=0.375$ m (see Fig.9(c)).

ii) when x_{cg} is in rearward position and the aero-brake is open, the capsule shows extra equilibrium points. For the "open satellite" configuration, two extra equilibrium points are located around $\alpha=70$ and 110 deg; equilibrium is unstable for the first angle, stable for the second one. The "open capsule" configuration shows only one extra equilibrium point around $\alpha=90$ deg. In this point equilibrium is unstable or stable, depending on whether $\alpha=90$ deg is approached from lower or higher angles of attack. As already said, according to Chen at al. [6], the presence of these extra statically stable equilibrium points could be dangerous. In fact, for the "open satellite" configuration, at $\alpha=110$ deg, the capsule could stabilize in a wrong attitude because the stagnation point would not lay on the nose and the module, containing the payload, would be exposed to the flow. The same occurs for the "open capsule" configuration when $\alpha=90$ deg is approached from higher angles of attack.

iii) the position of the gravity center along the capsule axis influences the equilibrium stability; the more advanced this position, the more stable the equilibrium.

iv) the influence of the aero-brake is stabilizing.

Tables 8(a), (b) and (c) quantify the stability level by means of the stability derivatives. The effect of the aero-brake increases the stability level by an order of magnitude.
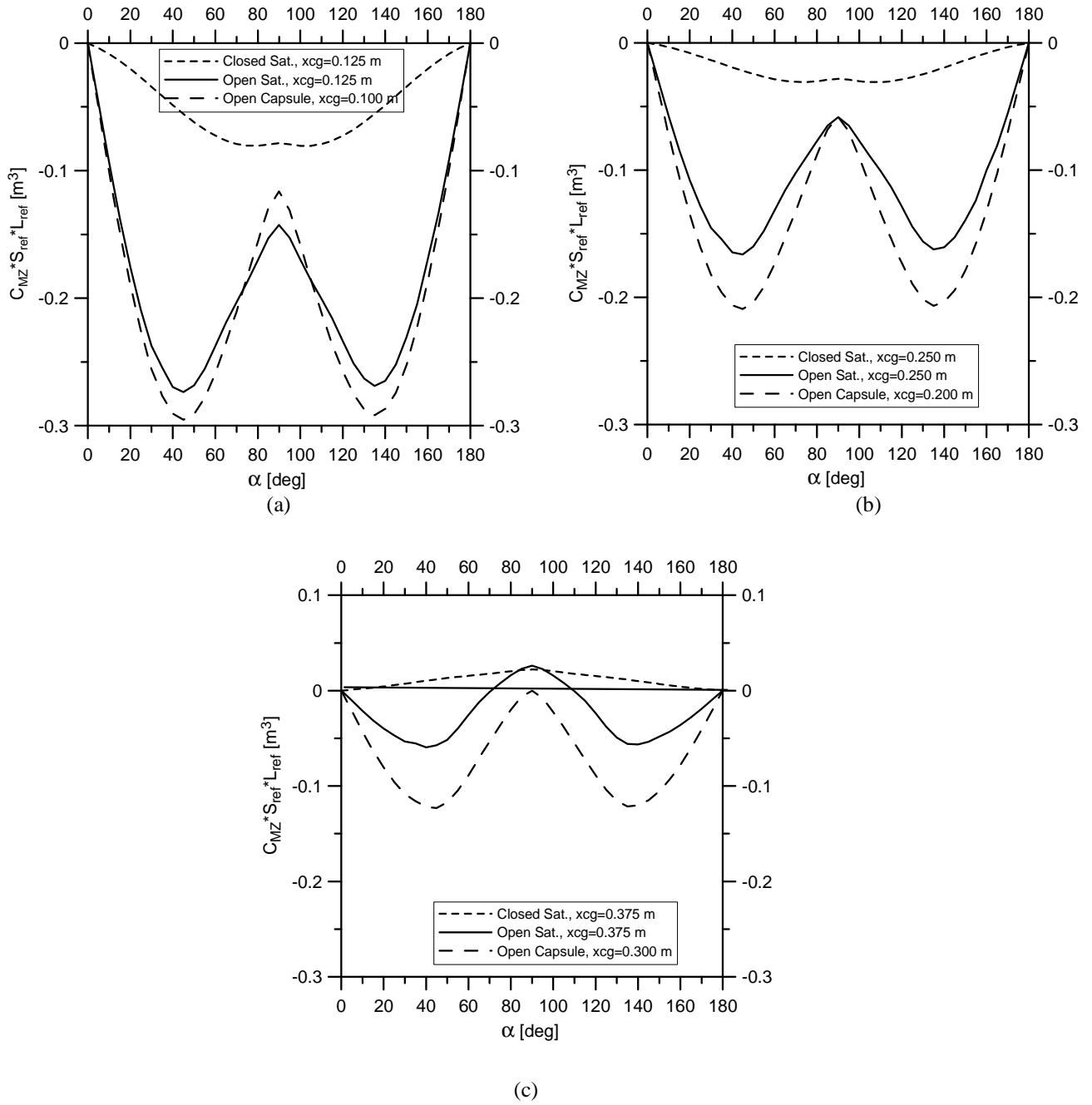
Fig.9 – Longitudinal moment (for less than dynamic pressure) as a function of the angle of attack for three reduction poles: (a) x_{cg}=0.125/0.100 m, (b) x_{cg}=0.250/0.200 m, (c) x_{cg}=0.375/0.300 m

Table 8(a): Stability derivatives for "closed satellite" configuration

Attitude	x_{cg}=0.125 m	x_{cg}=0.250 m	x_{cg}=0.375 m
FWD	-0.0009	-0.0004	0.0002
Medium FWD	//	//	//
Medium BCK	//	//	//
BCK	0.0009	0.0004	-0.0002

Table 8(b): Stability derivatives for "open satellite" configuration

Attitude	x_{cg}=0.125 m	x_{cg}=0.250 m	x_{cg}=0.375 m
FWD	-0.092	-0.0056	-0.0021
Medium FWD	//	//	0.0021
Medium BCK	//	//	-0.0020
BCK	0.089	0.0054	0.0019

Table 8(c): Stability derivatives for "open capsule" configuration

Attitude	x_{cg}=0.100 m	x_{cg}=0.200 m	x_{cg}=0.300 m
FWD	-0.0099	-0.0070	-0.0042
Medium FWD	//	//	0.0024
Medium BCK	//	//	-0.0026
BCK	0.0097	0.0069	0.0040

7. Conclusions and further developments

Deployable, or umbrella like, re-entry capsules, thanks to lightness and to low construction and management costs, seem to be a viable alternative to the current "conventional" capsules. The present authors already did successful computer tests, simulating the Earth re-entry and the Mars entry of such a kind of capsule.

Tests in the present paper are aimed at providing preliminary information about global parameters, such as drag coefficient and pitching moment, therefore at evaluating the longitudinal stability and local quantities such as heat flux and pressure. The present analysis also provides a preliminary altitude interval for the GPS black-out due to plasma frequency as well as preliminary information about the structural and thermal resistance of the fabric and of the support ribs. A more detailed analysis about the black-out, the thermal and structural resistance, as well as aeroelastic and vibrational effects has already been scheduled.

The 3-D tests verified that the capsule is longitudinally stable and the effect of the aero-brake increases the stability level by an order of magnitude.

8. References

[1] V. Carandente, G. Zuppardi, R. Savino, "Aerothermodynamic and stability analyses of a deployable reentry capsules, Acta Astronautica", **93**, 291-303 (2014)

[2] K. Yamada, T. Abe, K. Suzuki, D. Akita, O. Imamura, Y. Nagata, N.Honma. Reentry Demonstration of deployable and flexible aeroshell for future atmospheric entry vehicle using sounding rockets, 64th International Astronautical Conference, Naples (Italy) October 1-5 (2012)

[3] M. Iacovazzo, V. Carandente, R. Savino, G. Zuppardi, "Longitudinal Stability Analysis of a Suborbital Re-entry Demonstrator for a Deployable Capsule", Acta Astronautica, **106**, 101-110 (2015)

[4] G. Zuppardi, R. Savino, "DSMC Aero-Thermo-Dynamic Analysis of a Deployable Capsule for Mars Entry", presented at the International Workshop DSMC15, Sep. 13-17, Kauai, Hawaii USA (2015)

[5] D.L. Akin, "Applications of Ultra-Low Ballistic Coefficient Entry Vehicles to Existing and Future Space Missions", SpaceOps 2010 Conference, April 25-30, Huntsville, Alabama (2010)

[6] B. Chen, H. Zhan, W. Zhou. "Aerodynamic design of a re-entry capsule for high-speed manned re-entry", Acta Astronautica, **106**, 160-169 (2015)

[7] V. Carandente, R. Savino, M. Iacovazzo, C. Boffa, "Aerothermal Analysis of a Sample-Return Reentry Capsule", Tech Science Press FDMP, **9**, 461-484 (2013)

[8] M.W. Tauber, A Review of High Speed, Convective, Heat Transfer Computation Methods, NASA TP 2914 (1989)

[9] G. A. Bird, Molecular Gas Dynamics and Direct Simulation Monte Carlo, Clarendon Press, Oxford, Great Britain (1998).

[10] G. A. Bird, The DSMC Method, Version 1.1, Amazon, ISBS 9781492112907, Charleston, USA (2013)

[11] C. Shen, Rarefied Gas Dynamic: Fundamentals, Simulations and Micro Flows, Springer-Verlag, Berlin, Germany (2005)

[12] G.A. Bird, The DS2V Program User's Guide Ver. 4.5, G.A.B. Consulting Pty Ltd, Sydney, Australia (2008)

[13] G.A. Bird, The DS3V Program User's Guide Ver. 2.6, G.A.B. Consulting Pty Ltd, Sydney, Australia (2006).

[14] R.N. Gupta, J.M. Yos, R.A. Thompson, "A Review of Reaction Rates and Thermodynamic Transport Properties for an 11-Species Air Model for Chemical and Thermal Non-Equilibrium Calculations to 30,000 K", NASA TM 101528 (1989).

[15] G.A. Bird, Sophisticated Versus Simple DSMC, Proceedings of the 25th International Symposium on Rarefied Gas Dynamics, edited by M. Ivanov and A. Rebrov, Saint Petersburg, Russia (2006).

[16] G.A. Bird, M.A. Gallis, J.R. Torczynski, D.J. Rader, *Phys Fluid.* **21**, 017103 (2009).

[17] M.A. Gallis, J.R. Torczynski, D.J. Rader, G.A. Bird, *J. Comput. Phys.* **228**, 4532-4548 (2009)

[18] J.N. Moss, "Rarefied Flows of Planetary Entry Capsules", Special course on "Capsule Aerothermodynamics", Rhode-Saint-Genèse, Belgium, AGARD-R-808, 95-129, May 1995

[19] http://www.spacex.com/dragon

[20] B.D. Goldman, E. Dowell, "In-Flight Aeroelastic Stability of the Thermal Protection System on the NASA HIAD, Part II: Nonlinear Theory and Extended Aerodynamics", 56th AIAA/ASCE/AHS/ASC Structures, Structural Dynamics and Materials Conference, Kissimmee, Florida, USA (2015)

[21] S.C. Dixon, M.L. Hudson, "Flutter, Vibration and Buckling of Truncated Orthotropic Conical Shells with Generalized Elastic Edge Restraint", NASA TN D-5759 (1970)

[22] M. Kim, M. Keidar, I. Boyd, Analysis of an Electromagnetic Mitigation Scheme for Re-entry Telemetry Through Plasma, *J. Spacecraft and Rockets* **45**, 1223-1229 (2008)

Gennaro ZUPPARDI

Gennaro Zuppardi got a Laurea degree in Aeronautical Engineering in July 1976 (score: 110/110) at the University of Naples "Federico II".

He has been a lecturer in: 1) Fluid-dynamics at the University of Basilicata (a.y. 1993/94), 2) Experimental Fluid-dynamics at the University of Naples "Federico II" (a.y. 1994/95), 3) Hypersonic Aerodynamics at the University of Naples "Federico II", since a.y. 1997/98 up today.

Research activities: 1) Boundary layer diagnostics by non-intrusive technique (thermography), 2) Adaptive walls wind tunnel. 3) Aero-thermo-chemistry. 4) Rarefied Gas-Dynamics and DSMC, this subject is his current mayor.

He is author or co-author of 92 scientific papers and of a book in Hypersonic Aerodynamics.
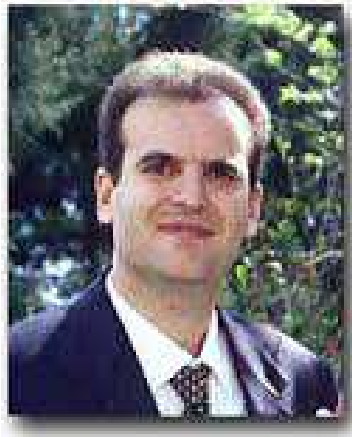
Raffaele SAVINO

Raffaele Savino, Ph.D., is professor of Aerodynamics at the University of Naples Federico II. He was responsible as of several research programs in collaboration with Research Centers and Space Agencies (ASI, CIRA, ESA, NASA). His memberships include the International Academy of Astronautics (IAA), the International Astronautical Federation (IAF), the Italian Association of Aeronautics and Astronautics (AIDAA), the American Institute of Aeronautics and Astronautics (AIAA). He is author of over 200 publications in the fields of Fluid Dynamics, Microgravity and Space Experimentation, Physics of Fluids, Hypersonic Aerodynamics, Heat transfer, Aerospace Propulsion Recent research activities include hypersonic numerical and experimental aerodynamics, aerothermochemistry, innovative heat pipes for ground and space applications, hybrid rocket propulsion.

Giuseppe MONGELLUZZO

Giuseppe Mongelluzzo is a student in Aerospace Engineering at the University of Naples "Federico II". He is currently involved in the study of the Aerothermodynamics of deployable re-entry capsules in rarefied flow field by means of Direct Simulation MonteCarlo codes. During his Laurea Thesis, he developed Rhinoceros CADs for capsules and ran 3-D (DS3V) and 2-D (DS2V) DSMC codes.